

Temporal Variations of Strength and Location of the South Atlantic Anomaly as Measured by *RXTE*

Felix Fürst^{a,b,*} Jörn Wilms^{a,b} Richard E. Rothschild^c
 Katja Pottschmidt^{c,d,e} David M. Smith^f
 and Richard Lingenfelter^c

^a*Dr. Karl-Remeis-Sternwarte, Sternwartstr. 7, 96049 Bamberg, Germany*

^b*Erlangen Centre for Astroparticle Physics, Erwin-Rommel-Straße 1, 91058 Erlangen, Germany*

^c*Center for Astrophysics and Space Sciences, University of California at San Diego, La Jolla, 9500 Gilman Drive, CA 92093-0424, USA*

^d*CRESST and NASA Goddard Space Flight Center, Astrophysics Science Division, Code 661, Greenbelt, MD 20771, USA*

^e*Center for Space Science and Technology, University of Maryland Baltimore County, 1000 Hilltop Circle, Baltimore, MD 21250, USA*

^f*SCIPP, University of California at Santa Cruz, 1156 High Street, Santa Cruz, CA 95064, USA*

Abstract

The evolution of the particle background at an altitude of ~ 540 km during the time interval between 1996 and 2007 is studied using the particle monitor of the High Energy X-ray Timing Experiment on board NASA's Rossi X-ray Timing Explorer. A special emphasis of this study is the location and strength of the South Atlantic Anomaly (SAA). The size and strength of the SAA are anti-correlated with the the 10.7 cm radio flux of the Sun, which leads the SAA strength by ~ 1 year reflecting variations in solar heating of the upper atmosphere. The location of the SAA is also found to drift westwards with an average drift rate of about $0.3^\circ/\text{yr}$ following the drift of the geomagnetic field configuration. Superimposed to this drift rate are irregularities, where the SAA suddenly moves eastwards and where furthermore the speed of the drift changes. The most prominent of these irregularities is found in the second quarter of 2003 and another event took place in 1999. We suggest that these events are previously unrecognized manifestations of the geomagnetic jerks of the Earth's magnetic field.

Key words: space radiation environment, South Atlantic Anomaly, radiation monitors, Rossi X-ray Timing Explorer

1 Introduction

Geomagnetically trapped ionized particles, mainly electrons and protons, are a hazard to modern spaceflight. They can cause failure of microprocessors aboard satellites, bias measurements of cosmic sources, and pose a health hazard to astronauts. In low-Earth orbits (LEO), at a height of several 100 km above the Earth's surface, a space vehicle encounters the most intense radiation in a region called the South Atlantic Anomaly (SAA; Kurnosova et al., 1962). In this region above the South Atlantic just off the Brazilian coast, the level of ionizing radiation can be increased by several orders of magnitude. This increase can be explained by a weakened magnetic field, which causes the geomagnetically trapped particles to mirror at lower altitudes, increasing the local particle flux (see, e.g., Evans, 2002). While the SAA is an extended region, it is common to define its position as the 2D-locus of the maximum of the local particle flux at a given altitude (Heynderickx, 1996).

1.1 *The Earth's magnetic field*

To a first crude approximation, the Earth's magnetic field can be modeled as a dipole with an axis that is offset from the Earth's center by about 500 km towards Southeast Asia and inclined by about 11 degrees with respect to the Earth's rotational axis (see Pinto et al., 1992). At a given altitude above the Earth's surface, in this approximation the weakest B -field is above the South Atlantic, the so-called South Atlantic Magnetic Anomaly (SAMA). While it is not a priori required that the local maximum of ionizing flux is located close to the minimum of the magnetic field, as its location also depends on the particle distribution in the atmosphere (Lauriente et al., 1996), there is a good correlation between the maximum of the ionizing flux and the B -field. The primary physical cause for the Earth's B -field is, however, dynamic currents in the outer core. These currents, consisting mainly of molten iron, produce

* Corresponding author.

Email addresses: `felix.fuerst@sternwarte.uni-erlangen.de` (Felix Fürst),
`joern.wilms@sternwarte.uni-erlangen.de` (Jörn Wilms),
`rrothschild@ucsd.edu` (Richard E. Rothschild),
`katja@milkyway.gsfc.nasa.gov` (Katja Pottschmidt), `dsmith@scipp.ucsc.edu`
(David M. Smith), `rlingenfelter@ucsd.edu` (and Richard Lingenfelter).

a self-sustaining dynamo which gives rise to the geomagnetic-field. The “Dynamo Theory” was first proposed by Elsasser (1946) to be applicable to the Earth. See Roberts and Glatzmaier (2000) for a review and a discussion of the stability of the dynamo. Despite the overall stability of the dynamo, the field configuration is slowly changing, giving rise to the secular variation of the field (see Malin, 1985, for a short historical review). From archeomagnetic data Pinto et al. (1992) have shown that the SAMA has been slowly drifting westwards for at least 1400 years. This long-term drifting was recently confirmed by Mandea et al. (2007), using data calculated via the GUFM model (Jackson et al., 2000) and the CHAOS model (model from the satellites *CHAMP*, *Ørsted* and *SAC-C*, Olsen et al., 2006). From time to time, however, an abrupt change in the secular variation is measured, which is called a “geomagnetic jerk”. These jerks occur when the fluid flows on the core surface change. Due to the complex nature of the geodynamo, such jerks are rather common. Jerks are found in geomagnetic data of the last century and show up as changes in the time derivative of the eastward-pointing component of the magnetic field. See Wardinski et al. (2008) and references therein for a description of the underlying physical processes.

1.2 *The particle environment*

In agreement with the SAMA location the maximum of the particle flux (SAA) is moving westwards as well. Because the aforementioned risks of high radiation to modern spaceflight make it necessary to know the location and strength of the SAA at any given time, a large number of measurements and investigations of this behavior have been carried out over the years. The constant change of the position of the SAA requires to monitor constantly the space environment and to develop models which predict the future movement of the SAA. Most of the previous works on the movement of the SAA compare recent measurements of the particle flux to the particle flux predicted by the *AP-8/AE-8* models. The *AP-8* model for protons was released in 1976 and includes all data taken after 1970 (Sawyer and Vette, 1976), while the *AE-8* for electrons was released in 1991 (Vette, 1991). Both models together include data from over 43 satellites (Barth et al., 2003). Nonetheless, these models are based on data taken with older instruments which were not necessarily as sophisticated as modern devices. With the help of these models, Konradi et al. (1994) and Badhwar et al. (1994) have shown that the SAA is located distinctly more westwards in modern measurements, leading to an average annual movement of about $0.3^\circ/\text{yr}$. The derived drift rate depends strongly on the accuracy of the models. Grigoryan et al. (2005) have shown that the SAA has somewhat different sizes and locations in different energy bands. This change of shape leads to a systematic error when comparing older models to recent measurements, which have been made using different de-

tectors. In an effort to compare measurements made with an identical setup, Badhwar (1997) compared data taken 21.2 years apart, on *Skylab* during December 1973 and January 1974 and on *Mir* in March 1995. He found a drift rate of $0.28 \pm 0.03^\circ/\text{yr}$ westward which is in very good agreement with other measurements.

Ginet et al. (2006) used a similar approach in comparing measurements taken between 2000 and 2006 with the Tri-Service Experiments Mission-5 (*TSX-5*) to 1994–1996 data from the Advanced Photovoltaic and Electronic Experiments (*APEX*), resulting in a somewhat faster movement of $0.43 \pm 0.13^\circ/\text{yr}$. The long average of the *TSX-5* mission might be responsible for that discrepancy (Ginet et al., 2006). Another indirect way to measure the particle flux is to record Single Event Upsets (SEU) or Single Event Effects (SEE) in electronic devices, see, e.g., Lauriente et al. (1996), Mullen et al. (1998) or Adolphsen et al. (1995). These measurements bear a higher systematic error, as the upsets can be caused by particles with different energies or even by cosmic rays. This uncertainty is reflected in the larger scatter of the derived movement rates, which vary between $0.19^\circ/\text{yr}$ and $0.4^\circ/\text{yr}$.

1.3 Long time measurement with *RXTE*

A shortcoming of all of these previous studies, however, is that since most of the measurements were taken with detectors on missions with a short lifetime, such as manned spacecraft, only pointwise data are available, even if they were made over a long range of time. This means that short time variations of the drift rate of the SAA had to be ignored. In this paper we study the SAA based on data from the *Rossi X-ray Timing Explorer (RXTE)*, taken continuously between 1996 and 2007. This is the first time that the SAA is studied on such a long and continuous data basis. In Sect. 2 we describe our detection method and our data extraction pipeline. In Sect. 4 our findings about the SAA are presented, with Sect. 4.1 focusing on the temporal evolution of the strength of the SAA and Sect. 4.2 concentrating on the location and the drift of the SAA. We summarize our results and discuss some future investigations in Sect. 5.

2 Instrumentation and data acquisition

2.1 The *Rossi X-ray Timing Explorer*

The presented analysis is based on data taken with instruments on the *Rossi X-ray Timing Explorer (RXTE)*, a satellite devoted to X-ray astronomy. *RXTE*

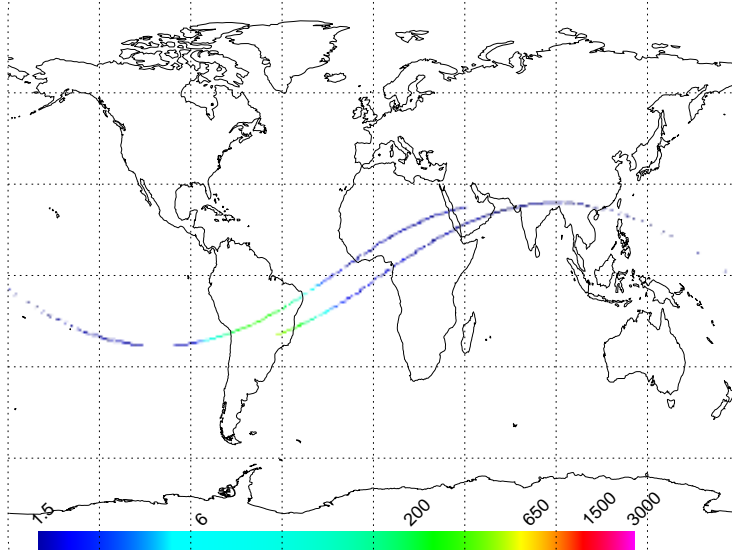


Fig. 1. Orbit and particle monitor rate of *RXTE* on 26 June 2005 from 00:06 h to 02:14 h in the altitude bin 490–499 km, showing $1\frac{1}{4}$ orbits. The scarce datapoints above the Pacific are due to the aforementioned orbital perturbations.

was launched on 1995 December 30 into a quasi-spherical orbit at an altitude of 592 km above the Earth. The orbital inclination is 23° and the orbital period is 90 min, such that the satellite passes directly through the SAA about 8 times a day on average. See Fig. 1 for a plot of the orbit of *RXTE* on June 26 2005 from 00:06 h to 02:14 h. The slight eccentricity of $e = 0.0008$ and orbital perturbations result in an altitude interval of ~ 30 km being covered by the satellite per orbit. Due to atmospheric drag, the satellite’s altitude is slowly decreasing, reaching 488 km in December 2007.

One of the three instruments on board *RXTE* is the High Energy X-ray Timing experiment¹ (HEXTE; Rothschild et al., 1998). HEXTE consists of two independent clusters of four NaI(Tl)/CsI(Na) phoswich scintillation counters, called HEXTE A and HEXTE B. The photomultiplier tubes attached to the scintillation counters are operated at a voltage of 845 V. As the photomultipliers can easily be damaged by exposure to energetic particles, the high-voltage is reduced to 220 V when passing through regions of increased background flux. In order to do so, the background in each cluster is constantly monitored using particle monitors consisting of a 1.27 cm diameter by 1.27 cm thick plastic scintillator cylinder and a 0.5 inch photomultiplier tube. One particle monitor is attached to each cluster (Fig. 2). The monitors are shielded by aluminum, providing a threshold energy of around 0.8 MeV for electrons and 17 MeV for protons. Due to slight differences in the radiation environment of the satellite, while the count rates from the two monitors show very similar

¹ <http://heasarc.gsfc.nasa.gov/docs/xte/HEXTE.html>

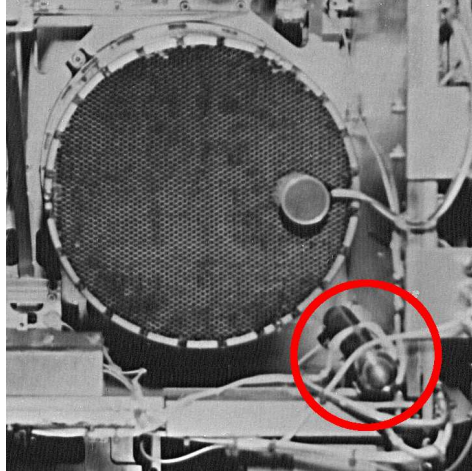


Fig. 2. Photograph of portion of a HEXTE cluster showing the collimator above one of four phoswich scintillation detectors. The particle monitor is located in the red circle in the lower right.

behavior, HEXTE A's rates are typically 2% larger than HEXTE B's rates (Fig. 4). In the later analysis, this offset was taken into account by introducing a multiplicative flux normalization constant in all fits and keeping all other parameters describing the shape of the SAA the same for both detectors.

Both monitors remain fully functional throughout the SAA passages. The count rate in each of the two particle background monitors is taken with a time resolution of 16 s and is available in the housekeeping data which are part of the standard *RXTE* data products. In this paper data taken between January 1996 and January 2008 are taken into account, corresponding to $\sim 23 \times 10^6$ data points in ~ 20100 individual housekeeping data files for each cluster. We therefore have detailed and quasi-uninterrupted background radiation measurements at *RXTE*'s altitude available for a time interval of 12 years. In terms of time coverage, these data represent one of the best statistics of the SAA region investigated up to date.

2.2 Mapping the SAA

In order to study the shape and location of the SAA, averaged particle flux maps were determined with a time resolution of 3 months and a spatial resolution of 0.25° in longitude, 0.5° in latitude, and 10 km in altitude. The grid resolution chosen is a compromise between the desire to obtain a good spatial resolution and a good signal to noise ratio in the resulting maps. In the southernmost latitude bins, which are closest to the center of the SAA and on which most of the following discussion is based, each bin represents the average of

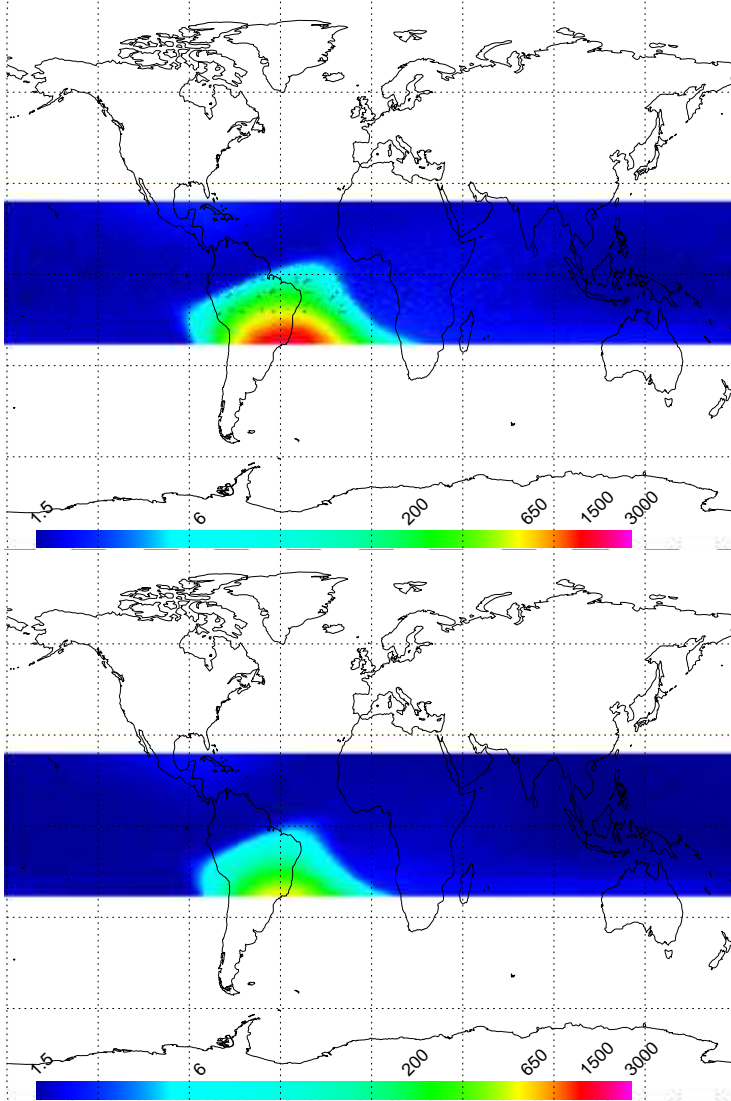


Fig. 3. Maps of the average count rate of the particle monitor of *HEXTE B*. *Top*: 1997, 1st quarter, altitude 570–579 km. *Bottom*: 2003, 3rd quarter, altitude 500–509 km.

at least 6 measurements. Towards the equator the number of measurements decreases. On average, each pixel is visited 1.5 times. Figure 3 shows two examples for the generated maps which show the countrate projected on the Earth. We have chosen the years 1997 and 2003 as examples as they provide good statistics and show the typical change of the SAA over the years.

As discussed in Sect. 2.1, atmospheric drag causes the satellite to constantly lose altitude. For this reason, the highest altitudes are only mapped in the first few years, while lower altitudes are only mapped more recently. To indicate this change, in this paper the different colors and symbols listed in Table 1 are used in all plots displaying the time dependence of an SAA related quantity. This approach allows us to check whether the general trends discussed in the

Table 1

Symbols and colors used in the plots. The last column gives the time-bins in years for which data for that specific altitude are available. Time-bins are 3 months in duration each.

Symbol	Color	Altitude (km)	Time-Bins
cross (+)	red	580–589	1996.00–1999.50
asterisk (*)	violet	570–579	1996.00–2000.25
diamond (◇)	orange	560–569	1996.00–2001.00
triangle (▲)	light blue	550–559	1999.50–2001.75
square (■)	green	540–549	2000.50–2002.00
times (×)	orange	530–539	2001.25–2002.75
cross (+)	green	520–529	2001.75–2003.25
asterisk (*)	red	510–519	2002.25–2004.50
diamond (◆)	dark blue	500–509	2002.75–2006.25
triangle (▲)	turquoise	490–499	2003.75–2007.75

next sections are altitude dependent. We note that while some properties of the SAA are altitude dependent (see, e.g., Ginet et al., 2006), in the following we will concentrate on the shape and position of the SAA, which have been shown to be independent of altitude (Grigoryan et al., 2005).

3 Methodology

The distribution of the particle flux with longitude has traditionally been described using Gaussian functions (e.g., Konradi et al., 1994; Bühler et al., 1996, and references therein), with the peak of the Gaussian describing the position of the SAA and its width being a measure for its size. A closer inspection of the particle monitor rates along one latitude bin reveals, however, that the SAA is distinctly asymmetric in shape (see Fig. 4). An asymmetric function is thus better suited to model the overall longitude-dependent particle flux. Numerical experimenting revealed that for all measurements described here a Weibull function (Weibull, 1951) defined by

$$y(x; A, k, \lambda, \theta) = \begin{cases} A \cdot \frac{k}{\lambda} \cdot \left(\frac{x-\theta}{\lambda}\right)^{k-1} \cdot \exp\left(-\left(\frac{x-\theta}{\lambda}\right)^k\right) & \text{for } x \geq \theta \\ 0 & \text{for } x < \theta \end{cases} \quad (1)$$

gives a significantly better description of the shape of the SAA in terms of the

χ^2 -value of the fits. Here, x is the geographic longitude and the fit parameters are A , the normalization (or strength), λ the scale parameter, θ the shift parameter, and k the shape parameter of the Weibull function. Weibull functions are applicable for a wide range of phenomena (see Brown and Wohletz, 1995, for an overview), but have to our knowledge not yet been used to describe the shape of the SAA. The Weibull function is normalized such that

$$\int_{-\pi}^{+\pi} y(x; A, k, \lambda, \theta) dx = A \quad (2)$$

i.e., the normalization A is proportional to the total longitude integrated particle flux. In the following, we will call A the strength or flux of the SAA.

The position of the maximum of the Weibull function, \bar{x} , is

$$\bar{x} = \lambda \cdot \left(\frac{k-1}{k} \right)^{\frac{1}{k}} + \theta \quad (3)$$

and the variance of this distribution, σ_{wei}^2 , is given by

$$\sigma_{\text{wei}}^2 = \lambda^2 \cdot \Gamma \left(1 + \frac{2}{k} \right) - \mu^2 \quad (4)$$

where $\Gamma(x)$ is the Gamma-function. To illustrate that a Weibull function indeed describes the data better than a simple Gaussian, Fig. 4 compares fits of both functions to data taken at -23° latitude early in the mission. With $\chi^2 = 4.39 \cdot 10^4$ and 2875 degrees of freedom, the best-fit Weibull function describes the data significantly better than a Gaussian function ($\chi^2 = 1.46 \cdot 10^5$, 2876 degrees of freedom). For times taken during the solar maximum later in the mission, the SAA shape becomes more symmetric and Gaussians describe the shape almost as well as the Weibull function. Even during those times, however, the Weibull fits consistently give lower χ^2 -values than Gaussian fits. In the following, we will therefore only present results from the Weibull fits. We note, however, that the main results presented in this paper are independent of the specific fit function employed and only differ in minor details.

To allow us to gauge the overall quality of the data modeling, Fig. 5 shows the χ^2 -values of the Weibull and Gaussian fits for the entire campaign. The quality of the fits is usually very good. The large values of the reduced χ^2 of around 8 can be ascribed to the fact that in the maximum of the latitude cut the data shows a detailed substructure which can not be well described by a simple smooth function such as a Weibull or a Gaussian. At the end of every altitude bin, the χ^2 -values decrease dramatically. This decrease is due

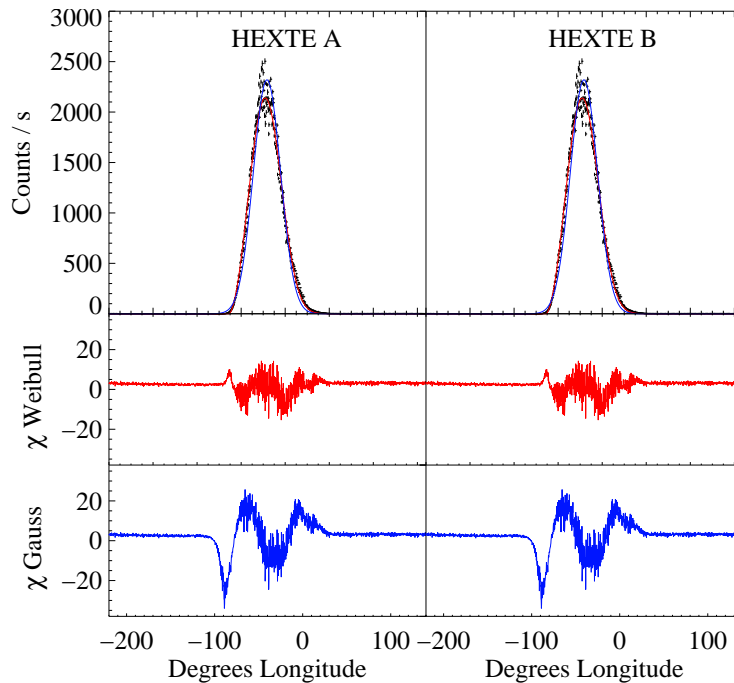


Fig. 4. Top: Simultaneous fit of HEXTE A (left panels) and B (right panels) monitor for 1997, 1st quarter, altitude 570 – 579 km and latitude -23° . Middle: Residuals of the best fit Weibull function (red curve in the top panel). Bottom: Residuals of the best fit Gaussian function (blue curve in the top panel).

to the fact that at the end of a bin only very few measurements are taken at that altitude, increasing the measurement uncertainty and thus decreasing χ^2 . Data points with $\chi^2 < 10^4$ were consequently not taken into account in the modeling described below.

4 Results: Evolution of the SAA 1996–2007

In this section we describe the results of our study of the evolution of the SAA through one solar cycle, from 1996 until the end of 2007. In our analysis, we concentrate on the southernmost tracks of *RXTE*, i.e., the HEXTE particle monitor count rate measured in the southernmost or the 11 southernmost latitude bins. In these bins the signal to noise ratio is highest. In addition, these bins are the ones closest to the center of the SAA and therefore most representative for its overall behavior. While we also performed some altitude dependent analysis, the main emphasis will be on the dependence of the strength of the particle flux in the SAA (Sect. 4.1) and on the motion of the SAA between 1996 and 2007 (Sect. 4.2).

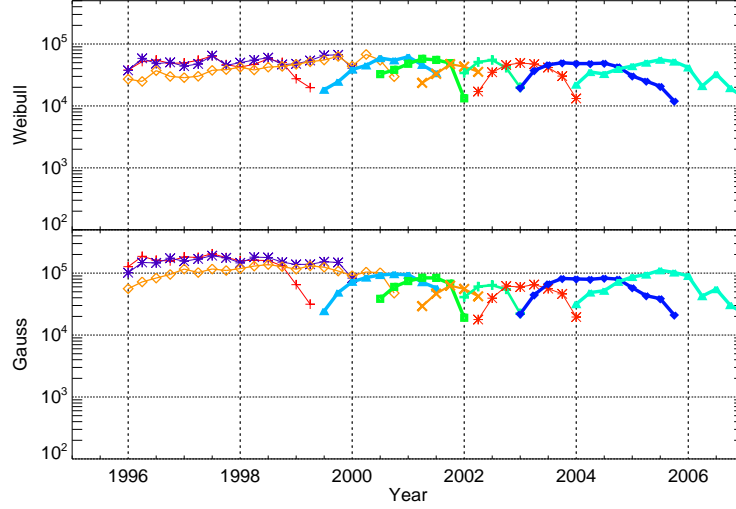


Fig. 5. χ^2 -values of the Weibull (top) and Gaussian (bottom) fit for the duration of the campaign. Fits have typically ~ 2500 degrees of freedom and were done for the southernmost latitude. The lower χ^2 -values at the start and end of each altitude bin interval are due to the sparseness of the data and therefore the larger error bars. See Table 1 for an explanation of the symbols used.

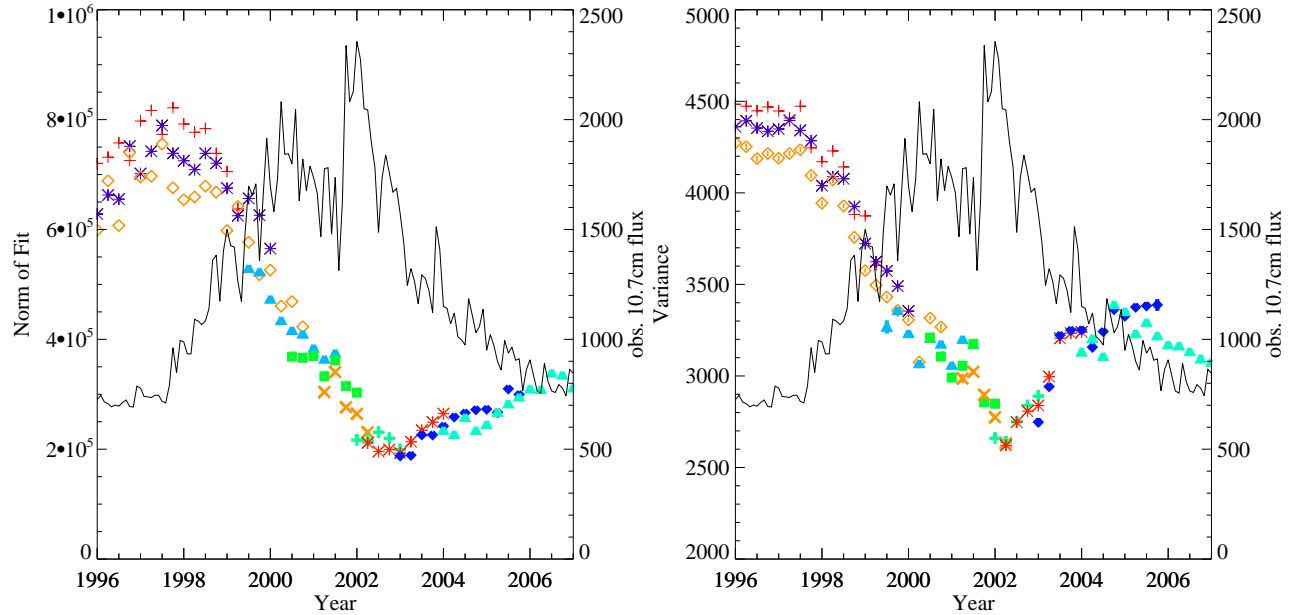


Fig. 6. Evolution of the strength and width of the SAA from 1996 to 2007 as parametrized by the normalization (left) and the variance (right) of the best fitting Weibull function. See Table 1 for an explanation of the symbols used. The black line shows the solar 10.7 cm radio flux.

4.1 Temporal Variation of the strength

Figure 6 shows the evolution of the normalization (A in Eqn. 1) and the variance for the Weibull fits from 1996 to 2007. These parameters are good

proxies for the evolution of the particle flux in the SAA during that time interval. As previously shown, e.g., by Bühler et al. (1996), Huston et al. (1996), and Dachev et al. (1999), both parameters are inversely correlated with the 10.7 cm radio flux from the Sun measured in $10^{-22} \text{ W m}^{-2} \text{ Hz}^{-1}$ (obtained by the National Geophysics Data Center²), which is a measure of the solar activity. As outlined by Huston et al. (1996) and Dachev et al. (1999), this inverse correlation is due to heating of the upper atmosphere during times of higher solar activity. This heating leads to a higher neutral density in the altitude region of the SAA and consequently to a higher absorption and deflection of trapped particles, which results in a lower particle flux compared to times of lower solar activity. A cross-correlation analysis shows a maximum of the absolute value of the cross correlation function of ~ 0.75 at a time delay of 1 year. This result is in agreement with Huston et al. (1996). This time lag between the particle flux as characterized by the normalization of the SAA and the solar 10.7 cm flux is also illustrated in Fig. 7 where we plot both quantities against each other. As the *RXTE* data are available for ~ 12 years, they cover one full 11 year solar cycle, and consequently lie on an ellipse as is characteristic for physical quantities exhibiting an hysteric behavior. A few outliers can be seen in Fig. 7 around 2001, which can be ascribed to a short term reduction of the solar 10.7 cm flux in this time window. The particle environment has damped out these short term fluctuation so that the 2001 data points do not fall perfectly onto the ellipse.

4.2 Movement of the SAA

To characterize the drift of the SAA we use the position of the maximum of the fits for the southernmost latitude bin. Figure 8 clearly shows a roughly linear motion in longitude, with a linear fit to the data resulting in a westerly motion of $0.248 \pm 0.003^\circ/\text{yr}$, which is in good agreement with results of other groups (see Badhwar, 1997, and references therein). In contrast to these earlier results, which were generally based on sparse data sampling, Fig. 8 clearly reveals significant deviations from the overall linear trend. Most obviously, a strong change in the position of the SAA is clearly visible between 2003 and 2004, where the SAA's center is moving towards the east, i.e., in the opposite direction of the usual movement. This behavior is seen in both, the Weibull and the Gaussian fits, and it is also present when considering not the maximum of the fits but the expectation value of the data. In addition, there is also no change in the quality of the Weibull or Gauss fits during that time (Fig. 5). The drift rates found in all of these approaches are very similar.

² The NGDC can be reached at <http://www.ngdc.noaa.gov>, the 10.7 cm data are available at ftp://ftp.ngdc.noaa.gov/STP/SOLAR_DATA/SOLAR_RADIO/FLUX/penticton.txt.

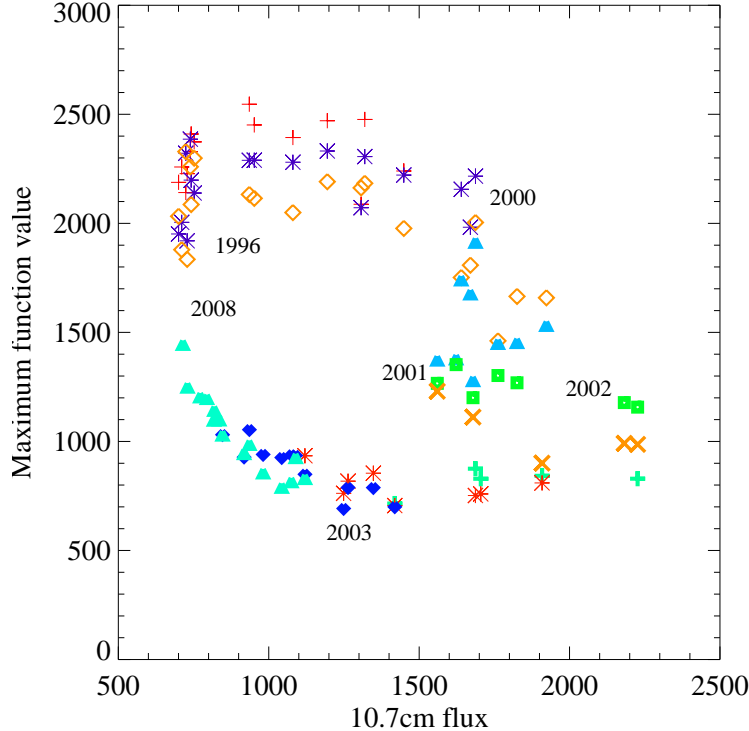


Fig. 7. The maximum value of the Weibull fit versus the solar 10.7 cm flux. The color code used is described in Table 1 and represents the altitude bins (and thus indirectly the time). The years indicate the approximate time of the data acquisition.

Since the signal to noise in the southernmost latitude bin is too low to allow a more detailed analysis of the drift of the SAA, we averaged the maximum position over the 11 southernmost latitude bins. All of these bins are still close to the maximum of the SAA and the latitude dependence of the particle count rate is very similar. Figure 9 shows that the averaged position shows the same behavior as the position for latitude 23° south only. This means that the sudden change between 2003 and 2004 is a persistent feature and is independent of latitude. A linear fit leads to a movement rate of $0.290 \pm 0.002^\circ/\text{yr}$. The residuals of this fit clearly show that in addition to the jump around 2003 another change of slope is apparent in 1998 (these residuals are also present in Fig. 8, but are only of borderline significance in these data).

Since a simple linear fit is not a good approximation to the movement of the SAA due to the sudden change in the movement in 1998 and 2003, we next parametrized the data by fitting it with piecewise linear functions, allowing for two “jumps” in the data. This approach gives a good description of the overall data, with the slope changing from $0.656(11)^\circ/\text{yr}$ for the time interval before 1998.25, to $0.346(5)^\circ/\text{yr}$ for the interval 1998.25–2003.25, and $0.467(12)^\circ/\text{yr}$ since then (Fig. 10). We note that with $\chi^2 = 2040.78$ for 104 degrees of freedom, this fit is significantly better than a fit in which the 1998.25-break is ignored. In the latter case, $\chi^2 = 2527.8$. Using the F -test to test the reasonability of the second break point of the linear fit gives a very low probability

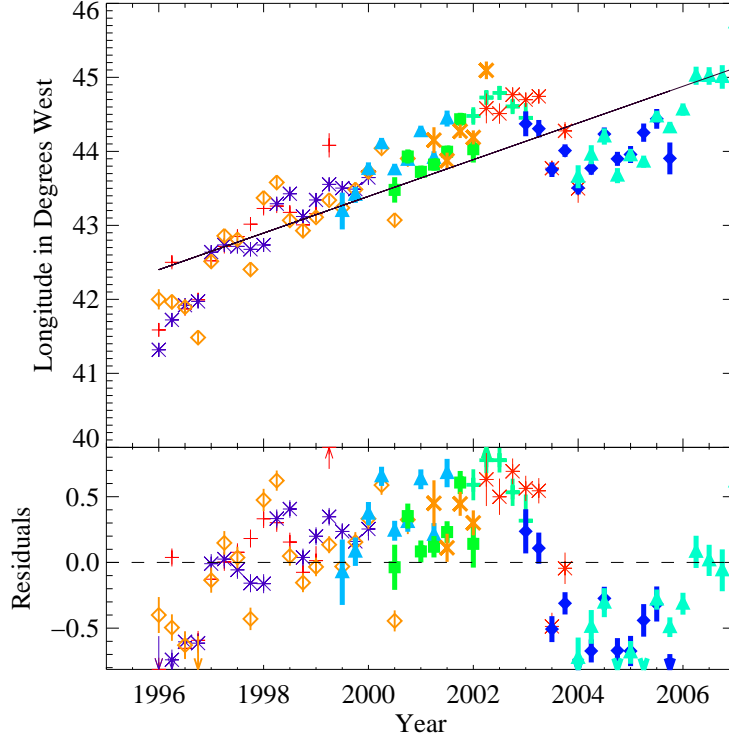


Fig. 8. Position of the maximum of the Weibull fit for latitude -23° and a linear fit to these data with a slope of $0.248(3)^\circ/\text{yr}$.

value of $4.065 \cdot 10^{-6}$ for the break to be a random artifact. Fits for the other ways used to determine the maximum of the SAA as discussed above lead to the same dates for the break points.

To determine the start and end of the change more precisely, we extracted the *RXTE* data again with a higher temporal resolution of 1 month. It was necessary to average over all altitudes to retain a good signal to noise ratio. This approach is justified since our previous studies confirm prior investigations showing that the position of the maximum of the SAA does not depend on the altitude for the small altitude range considered here (Grigoryan et al., 2005). Figure 11 shows the position of the maximum of the Weibull fit with a resolution of 1 month. Superposed to the data is again a piecewise linear fit in which the slope is allowed to change at two different dates. A χ^2 -minimization shows that the changes in slope occurred in February 2003 and in April 2004. The SAA region was therefore moving opposite to its usual direction of movement for slightly more than 1 year. With a movement rate of $1.14 \pm 0.094^\circ/\text{yr}$ eastwards, the SAA moved significantly faster than usual. The feature in 1999, which was found in the altitude dependent data, is still seen weakly in the high time resolution data. The backwards drift was distinctly shorter than the one in 2003, however, and thus the duration of the event cannot be determined.

We conclude that a sudden change in the movement of the SAA seems not to be rare, it is only the amplitude of the 2003.25-move that seems to be special.

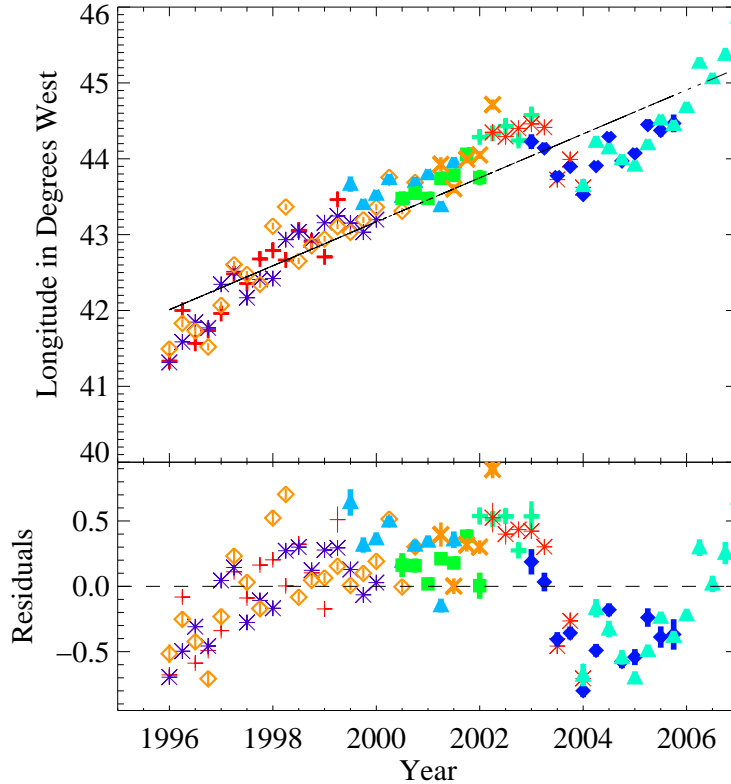


Fig. 9. Average position of the maximum of the Weibull fits for the data between latitude -23° and -18° . Superposed to the data is a linear fit to the data with a slope of $0.290(2)^\circ/\text{yr}$.

A sudden change means that the SAA moves quickly towards the east, during the third quarter of 2003 by as much as about 0.8° . Additionally the rate of the movement is different after each discontinuity. The commonly assumed rate of $0.3^\circ/\text{yr}$ seems to be valid only on longer timescales. On shorter timescales the rate can differ drastically from this value.

5 Summary and conclusion

Using the particle monitor aboard *RXTE* we have studied almost 12 years of continuously taken data of the radiation background in the low Earth orbit of this satellite. While the measurements could not determine the spectrum of the particle radiation, they allowed a detailed study of the shape and position of the SAA. We have shown that the shape of the SAA along one latitude can be better described by a Weibull function than by a pure Gaussian. The data show a clear anti-correlation between the 10.7 cm solar flux and the intensity and size of the SAA, with a lag of about 1 year. The large time range of our data allowed us to monitor the SAA for one solar cycle and we could show that after approximately 11 years the particle flux in the SAA has about the

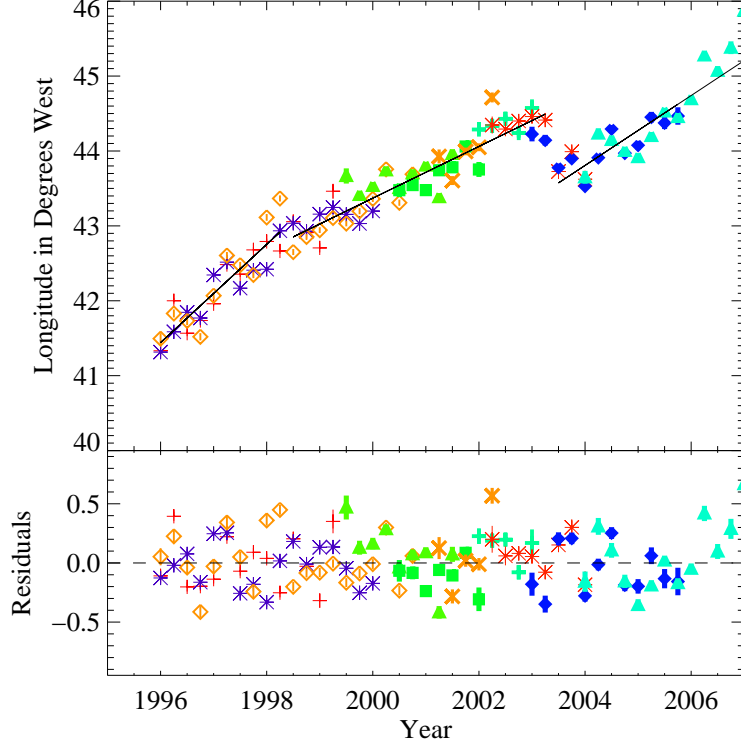


Fig. 10. Average position of the maximum of the Weibull fits for the data between latitude -23° and -18° . Superposed are three linear fits, with a slope of $0.65(1)^\circ/\text{yr}$ (1996.0–1998.25), $0.346(5)^\circ/\text{yr}$ (1996.5–2003.25), and $0.46(1)^\circ/\text{yr}$ (2003.5–2007.0), respectively.

same strength again.

The most important result of this study was that the location of the maximum of the fit as a function of time could be determined with a time resolution of a few months for the whole 12 years of data. The *RXTE* data confirm earlier measurements of a westward drift of the SAA, with a rate of $\sim 0.27^\circ/\text{yr}$, depending on what parametrization is chosen for its shape. The data also show, however, that the drift rate is not constant, but shows two irregularities, meaning that its position shifts slightly eastwards and then continues to move westwards. These break points were determined to be during the first quarter of 1998 and in the second quarter of 2003, with the latter one being distinctly stronger than the first one.

These irregularities could indicate a change in the particle population of the SAA. There are several phenomena which can produce such a change. On shorter timescales, solar coronal mass ejections (CME) can cause geomagnetic storms (Brueckner et al., 1998) and inject electrons and protons into the atmosphere. Asikainen and Mursula (2005) have shown that during the great storm of March 21, 2001 electrons became trapped in the SAA and drifted around the Earth together with the SAA. In November 2003 a major CME caused an intense geomagnetic storm, investigated by Becker-Guedes et al. (2007).

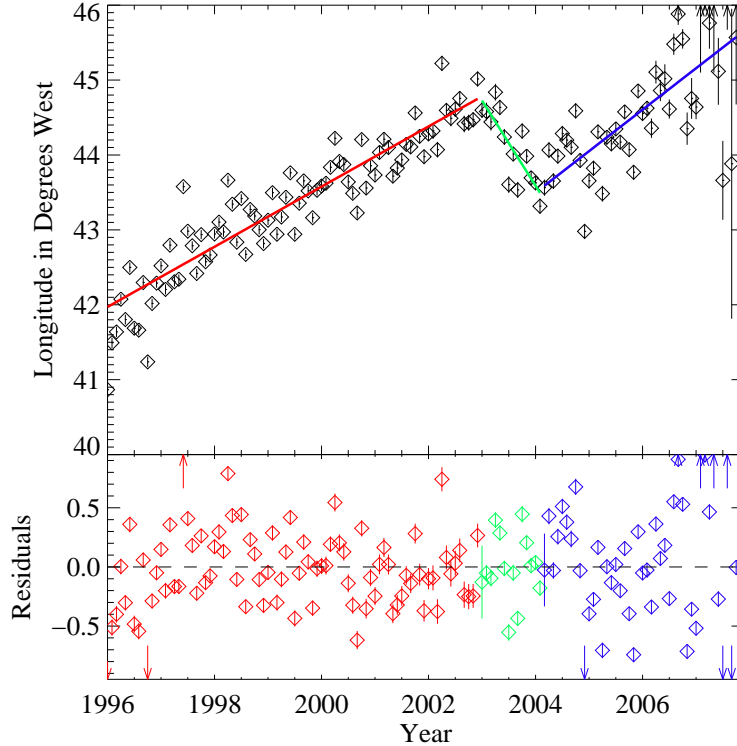


Fig. 11. Position of the maximum of the Weibull fit for latitude -23° and the best-fit piecewise linear function describing the motion of the SAA during the 2003 geomagnetic jerk. The second panel shows the residuals of the fit, with colors indicating the three parts of the fit.

While coincident with the time interval of the jump reported here, the jump started significantly earlier than the CME. Furthermore, the injected electrons that were seen in 2001 decay with a lifetime of only about 8 hours (Asikainen and Mursula, 2005), while the feature seen in the SAA has a longer lasting influence. These facts make it highly unlikely that CMEs are responsible for the measured irregularities.

As CMEs are the most prominent outside source which disturbs the geomagnetic field and the particle population around the Earth and only have a short term effect on the SAA, it is more likely that the origin for the changes in the movement is not in the particle distribution, but rather in the field itself. The most probable features of the field responsible for such events are the “geomagnetic jerks”. As described by Olsen and Manda (2007a), in early 2003 a large geomagnetic jerk occurred. This jerk might even have had an influence on the drift of the north magnetic dip pole, which accelerated for over 10 years but started to decelerate in 2003 (Olsen and Manda, 2007b). This result shows that the jerk had a major influence on the magnetic field of the Earth. Olsen and Manda (2008) furthermore analyzed satellite based geomagnetic data and could explain the observed accelerations in the secular variation via a relaxed tangentially geostrophic flow model. They found that the core flows

can fluctuate on time-scales of a few months, giving rise to equally fast changes in the geomagnetic field. It is likely that such changes could also influence the movement and the location of the SAA as these features depend strongly on the magnetic field. The timescales given by Olsen and Mandaia (2008) agree well with our data. We note that another, but weaker, geomagnetic jerk occurred in 1999 (Mandaia et al., 2000), right around the time of the earlier change in slope of the SAA drift discussed here.

We do not know of any jerk or other magnetic distortion which took place in early 2004 to account for the resumption of the westward drift of the SAA, although Olsen and Mandaia (2008) noticed a strong variation in the field at the end of 2004. These variations, however, seem to occur distinctly later than the reversal of the direction of the drift. Nonetheless the eastward drift could be connected to the jerk in 2003 and the duration of the eastward movement might be just showing the slow response of the trapped particles in the atmosphere.

This paper presented mainly observational data and a concluding physical explanation is beyond its scope. To analyze the proposed connection between jerks and the location of the SAA in further detail, additional data are clearly required. We are currently in the process of reducing data from the “Reuven Ramaty High Energy Solar Spectroscopic Imager” (*RHESSI*), which was launched shortly before the 2003 geomagnetic jerk. The instruments on this satellite have a higher time resolution than those on *RXTE* and also allow one to distinguish between electrons and protons. Hajdas et al. (2004) have shown that *RHESSI* is very capable of investigating the SAA region. In addition, data from the “Detection of Electro-Magnetic Emissions Transmitted from Earthquake Regions” satellite (*DEMETER*), which was launched in 2004, will become available. While *DEMETER* could not measure the 2003 geomagnetic jerks and its influences on the trapped radiation, it passes fully through the SAA. A map demonstrating the capability of *DEMETER* has been published by Sauvaud et al. (2008), which shows the SAA clearly. Additionally to the available geophysics satellites, other high-energy astronomy satellites such as *XMM-Newton* or *INTEGRAL* have particle detectors on board which will allow to study the evolution of the Earth’s magnetosphere and to provide independent measurements of the particle background on a long timescale.

Acknowledgements

We acknowledge partial support from Deutsches Zentrum für Luft- und Raumfahrt grants 50OR8080 and 50QR0801, from National Aeronautics and Space Administration grant NAG5-30720, and from Deutscher Akademischer Aus-

tauschdienst travel grant D/06/29438. We thank the complete *RXTE* team, especially the HEXTE team, for their support. We also thank the referees for their very helpful comments.

References

- Adolphsen, J., Barth, J. L., Stassinopoulos, E. G., Gruner, T., Wennersten, M., LaBel, K. A., Seidleck, C. M., Dec. 1995. Single Event Upset Rates on 1 Mbit and 256 Kbit Memories: CRUX Experiment on APEX. *IEEE Trans. Nuc. Sci.* 42 (6), 1964–1974.
- Asikainen, T., Mursula, K., Aug. 2005. Filling the South Atlantic anomaly by energetic electrons during a great magnetic storm. *Geophys. Res. Lett.* 32, 16102.
- Badhwar, G. D., Feb. 1997. Drift rate of the South Atlantic Anomaly. *J. Geophys. Res.* 102, 2343–2350.
- Badhwar, G. D., Konradi, A., Braby, L. A., Atwell, W., Cucinotta, F. A., Oct. 1994. Measurements of trapped protons and cosmic rays from recent shuttle flights. *Adv. Space Res.* 14, 67–72.
- Barth, J. L., Dyer, C. S., Stassinopoulos, E. G., Jun. 2003. Space, Atmospheric, and Terrestrial Radiation Environments. *IEEE Trans. Nuc. Sci.* 50 (3), 466–482.
- Becker-Guedes, F., Sahai, Y., Fagundes, P. R., Espinoza, E. S., Pillat, V. G., Lima, W. L. C., Basu, S., Basu, S., Otsuka, Y., Shiokawa, K., MacKenzie, E. M., Pi, X., Bittencourt, J. A., May 2007. The ionospheric response in the Brazilian sector during the super geomagnetic storm on 20 November 2003. *Ann. Geophys.* 25, 863–873.
- Brown, W. K., Wohletz, K. H., Aug. 1995. Derivation of the Weibull distribution based on physical principles and its connection to the Rosin-Rammler and lognormal distributions. *J. App. Phys.* 78, 2758–2763.
- Brueckner, G. E., Delaboudiniere, J.-P., Howard, R. A., Paswaters, S. E., St. Cyr, O. C., Schwenn, R., Lamy, P., Simnett, G. M., Thompson, B., Wang, D., 1998. Geomagnetic storms caused by coronal mass ejections (CMEs): March 1996 through June 1997. *Geophys. Res. Lett.* 25, 3019–3022.
- Bühler, P., Desorgher, L., Yehnder, A., Daly, E., Adams, L., 1996. Observations of the low earth orbit radiation environment from MIR. *Radiat. Meas.* 26 (6), 917–921.
- Dachev, P., Tomov, B. T., Matviichuk, Y. N., Koleva, R. T., Semkova, J. V., Petrov, V. M., 1999. Solar cycle of MIR radiation environment as observed by the LIULIN dosimeter. *Rad. Meas.* 30, 269–274.
- Elsasser, W. M., Feb. 1946. Induction Effects in Terrestrial Magnetism Part I. Theory. *Phys. Rev.* 69, 106–116.
- Evans, S. W., 2002. Space environment hazards. In: 43rd Structures, Structural

- Dynamics, and Materials Con. AIAA/ASME/ASCE/AHS/ASC, AIAA, Reston, pp. 1610–1616.
- Ginet, G. P., Thompson, T., Madden, D., Easley, S. M., Dec. 2006. Energetic Proton Maps for the South Atlantic Anomaly. AGU Fall Meeting Abstracts, A1359.
- Grigoryan, O. R., Petrov, A. N., Romashova, V. V., 2005. On the Drift of the South Atlantic Anomaly. In: WDS '05 Proceedings of Contributed Papers. Vol. 2. Matfyzpress, Prague, pp. 251–256.
- Hajdas, W., Eggel, C., Wigger, C., Sanctuary, H., Zehnder, A., Smith, D., Oct. 2004. Spacecraft Activation and South Atlantic Anomaly Profiles Measured with RHESSI Satellite. In: Fletcher, K. (Ed.), Proc. Radiation and its Effects on Components and Systems, RADECS 2003. ESA SP-536. ESA Publications Division, Noordwijk, pp. 607–610.
- Heynderickx, D., 1996. Comparison between methods to compensate for the secular motion of the South Atlantic Anomaly. *Rad. Meas.* 26 (3), 369–373.
- Huston, S. L., Kuck, G. A., Pfitzer, K. A., 1996. Low Altitude Trapped Radiation Model Using TIROS/NOAA Data. In: Lemaire, J. F., Heyndericks, D., Baker, D. N. (Eds.), *Radiation Belts: Models and Standards*. AGU Geophysical Monograph 97, AGU, Washington, pp. 119–122.
- Jackson, A., Jonkers, A., Walker, M., 2000. Four centuries of geomagnetic secular variation from historical records. *Philosophical Transactions of the Royal Society, London* 358, 957–990.
- Konradi, A., Badhwar, G. D., Braby, L. A., Oct. 1994. Recent space shuttle observations of the South Atlantic anomaly and the radiation belt models. *Adv. Space Res.* 14, 911–921.
- Kurnosova, L. V., Kolobyanina, T. N., Logachev, V. I., Razorenov, L. A., Sirotkin, I. A., Fradkin, M. I., Aug. 1962. Discovery of radiation anomalies above the South Atlantic at heights of 310–340 km. *Planet. Space Sci.* 9, 513–516.
- Lauriente, M., Vampola, V. L., Gosier, K., 1996. Experimental Validation fo South Atlantic Anomaly Motion Using a Two-Dimensional Cross-Correlation Technique. In: Lemaire, J. F., Heyndericks, D., Baker, D. N. (Eds.), *Radiation Belts: Models and Standards*. AGU Geophysical Monograph 97, pp. 109–117.
- Malin, S. R. C., Sep. 1985. On the unpredictability of geomagnetic secular variation. *Physics of the Earth and Planetary Interiors* 39, 293–296.
- Mandea, M., Bellanger, E., Le Mouél, J.-L., Dec. 2000. A geomagnetic jerk for the end of the 20th century? *Earth Planet. Sci. Lett.* 183, 369–373.
- Mandea, M., Korte, M., Mozzoni, D., Kotzé, P., 2007. The magnetic field changing over the southern African continent: a unique behaviour. *South African Journal of Geology* 110, 2-3, 193–202.
- Mullen, E. G., Ginet, G., Gussenhoven, M. S., Madden, D., 1998. SEE Relative Probability Maps of Space Operations. *IEEE Trans. Nuc. Sci.* 45 (6), 2954–2963.
- Olsen, N., Lühr, H., Sabaka, T. J., Mandea, M., Rother, M., Tøffner-Clausen,

- L., Choi, S., Jul. 2006. CHAOS—a model of the Earth’s magnetic field derived from CHAMP, Ørsted, and SAC-C magnetic satellite data. *Geophysical Journal International* 166, 67–75.
- Olsen, N., Manda, M., Mar. 2007a. Investigation of a secular variation impulse using satellite data: The 2003 geomagnetic jerk. *Earth Planet. Sci. Lett.* 255, 94–105.
- Olsen, N., Manda, M., Jul. 2007b. Will the Magnetic North Pole Move to Siberia? *EOS Transactions* 88, 293–293.
- Olsen, N., Manda, M., Jun. 2008. Rapidly changing flows in the Earth’s core. *Nature Geoscience* 1, 390–394.
- Pinto, Jr., O., Gonzalez, W. D., Pinto, I. R. C. A., Gonzalez, A. L. C., Mendes, Jr., O., 1992. The South Atlantic Magnetic Anomaly: Three Decades of Research. *J. Atmos. Terrest. Phys.* 54 (9), 1129–1134.
- Roberts, P. H., Glatzmaier, G. A., Oct. 2000. Geodynamo theory and simulations. *Rev. Modern Phys.* 72, 1081–1123.
- Rothschild, R. E., Blanco, P. R., Gruber, D. E., Heindl, W. A., MacDonald, D. R., Marsden, D. C., Pelling, M. R., Wayne, L. R., Hink, P. L., Mar. 1998. In-Flight Performance of the High-Energy X-Ray Timing Experiment on the Rossi X-Ray Timing Explorer. *Astrophys. J.* 496, 538.
- Sauvaud, J.-A., Maggiolo, R., Jacquy, C., Parrot, M., Berthelier, J.-J., Gamble, R. J., Rodger, C. J., May 2008. Radiation belt electron precipitation due to VLF transmitters: Satellite observations. *Geophys. Rev. Lett.* 35, 9101.
- Sawyer, D. M., Vette, J. I., Dec. 1976. AP-8 trapped proton environment for solar maximum and solar minimum. NASA STI/Recon Technical Report N 77, 18983.
- Vette, J. I., Nov. 1991. The AE-8 trapped electron model environment. NASA STI/Recon Technical Report N 92, 24228.
- Wardinski, I., Holme, R., Asari, S., Manda, M., Mar. 2008. The 2003 geomagnetic jerk and its relation to the core surface flows. *Earth Planet. Sci. Lett.* 267, 468–481.
- Weibull, W., 1951. A statistical distribution function of wide applicability. *J. Appl. Mech.-Trans. ASME* 18(3).